

# Exploiting anisotropic particle shape to electrostatically assemble colloidal molecules with high yield and purity

Yogesh Shelke<sup>a</sup>, Susana Marín-Aguilar<sup>b</sup>, Fabrizio Camerin<sup>b</sup>, Marjolein Dijkstra<sup>b</sup>, Daniela J. Kraft<sup>a,\*</sup>

<sup>a</sup>*Soft Matter Physics, Huygens-Kamerlingh Onnes Laboratory, Leiden University, PO Box 9504, 2300 RA Leiden, The Netherlands*

<sup>b</sup>*Soft Condensed Matter, Debye Institute for Nanomaterials Science, Utrecht University, Princetonplein 1, 3584 CC Utrecht, The Netherlands*

---

## 1 Parking algorithm based on random adsorption

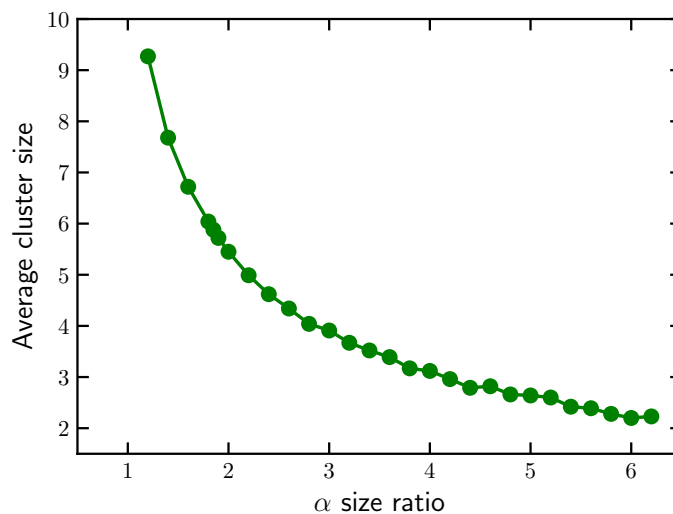


Figure S1: Average cluster size as a function of size ratio  $\alpha$  as obtained from the random parking algorithm based on random adsorption of spheres onto the surface of a cube.

In Figure S1, we show the average cluster size as a function of size ratio  $\alpha = \sigma_s/\sigma_c$  for the random parking algorithm based on the random adsorption of spheres with diameter  $\sigma_s$  onto the surface of a cube with edge length  $\sigma_c$ , as described in the Methods section. We note that the

---

\*Corresponding author  
Email address: [kraft@physics.leidenuniv.nl](mailto:kraft@physics.leidenuniv.nl) (Daniela J. Kraft)

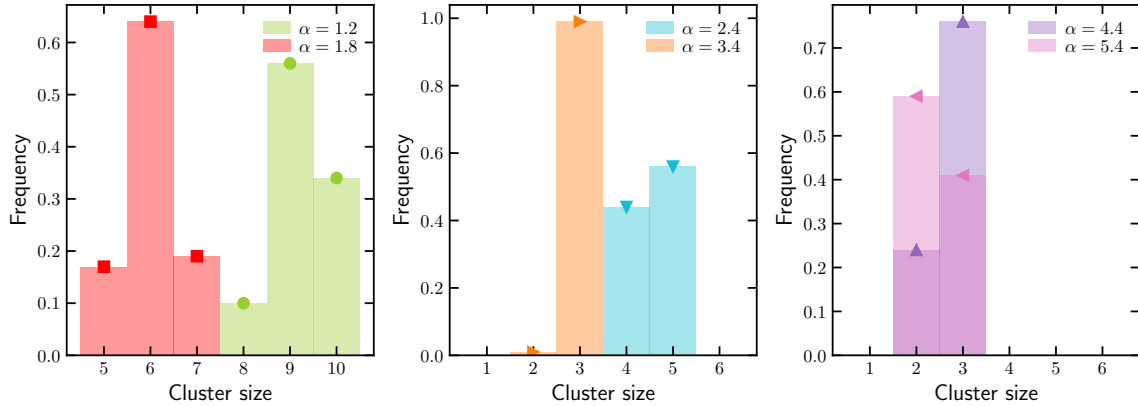


Figure S2: Cluster size distributions as obtained from the random parking algorithm based on random adsorption of spheres onto the surface of a cube for different size ratios  $\alpha$ .

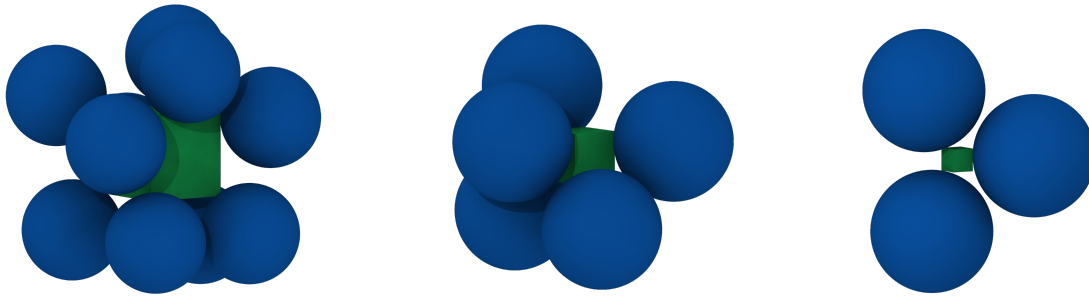


Figure S3: Typical configurations as obtained from the random parking algorithm based on random adsorption of spheres onto the surface of a cube for different size ratios  $\alpha = 1.2, 2.4$  and  $5.4$ .

average cluster size, defined as the average number of particles attached to the cube, is higher than in experiments and Monte Carlo simulations. Analyzing the resulting clusters as obtained from the random adsorption parking algorithm, we observe a tendency of satellite particles to be adsorbed onto the edges and corners of the cubes rather than the faces, leading to more free space for other satellite particles to be bounded and thus to higher averaged numbers of bounded spheres. In addition, we show cluster size distributions in Figure S2, which appear to be broader and shifted towards higher numbers of bound spheres than the ones reported in the main text for Monte Carlo simulations. Even the highest size ratio  $\alpha$  shows a broader distribution, where not only clusters of two but also of three bound satellite spheres could be observed. In Figure S3, we display typical

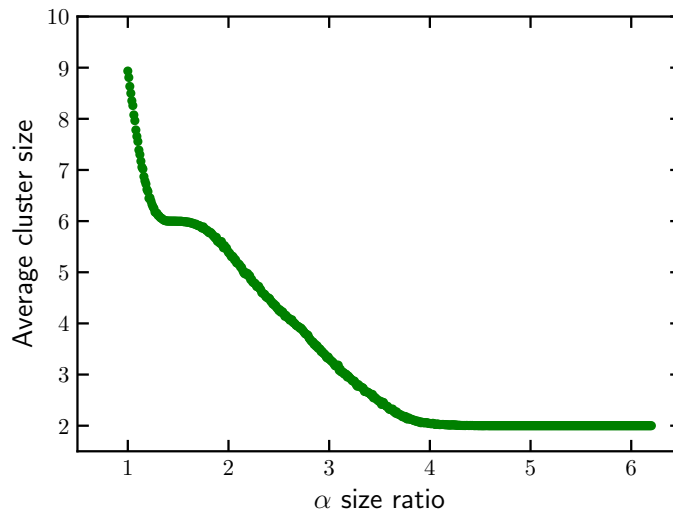


Figure S4: Average cluster size as a function of size ratio  $\alpha$  as obtained from the random parking algorithm based on selecting a random site for spheres attached to the surface of a cube.

configurations as obtained using the random adsorption parking algorithm for varying size ratios.

## 2 Parking algorithm based on selecting a random site

In Figure S4, we report the average cluster size for different size ratios  $\alpha = \sigma_s/\sigma_c$  for the random parking algorithm based on selecting a random site for a sphere with diameter  $\sigma_s$  on the surface of a cube with edge length  $\sigma_c$ , as described in the Methods section. The average cluster sizes fully resemble the ones reported in the main text for the experiments and the Monte Carlo simulations using screened Coulomb potentials for the interactions. The cluster size distributions, shown in Figure S5, also resemble the ones extracted from Monte Carlo simulations and the experimental ones. This confirms the preference of the spheres to be located on the faces of the cube, as the probability to select a random position at one of the faces is higher than selecting a random site on one of the edges or corners of the cube. Therefore, the difference in cluster size distribution found with the random adsorption parking algorithm is due to the fact that the minimum distance condition between the surface of a cube and a sphere is enforced. Representative configurations for the random site parking algorithm are reported in Figure S6.

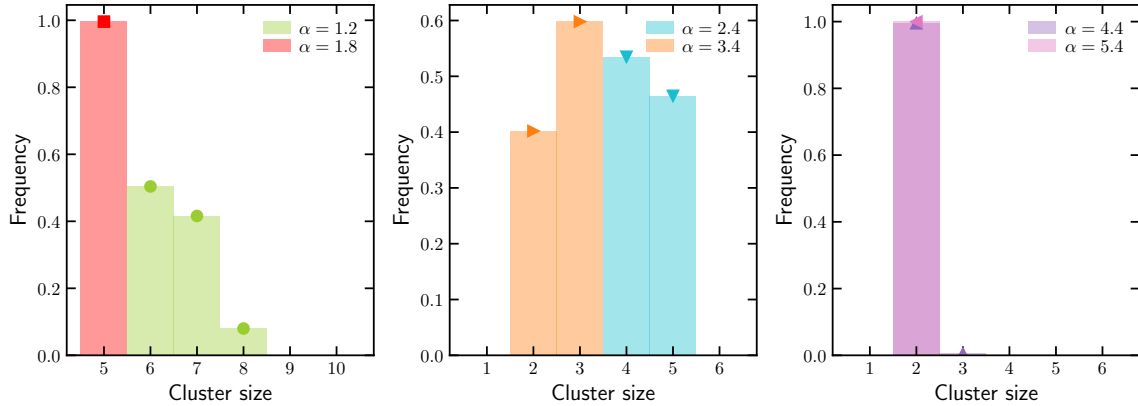


Figure S5: Cluster size distributions as obtained from the random parking algorithm based on selecting a random site for spheres attached to the surface of a cube for different size ratios  $\alpha$ .

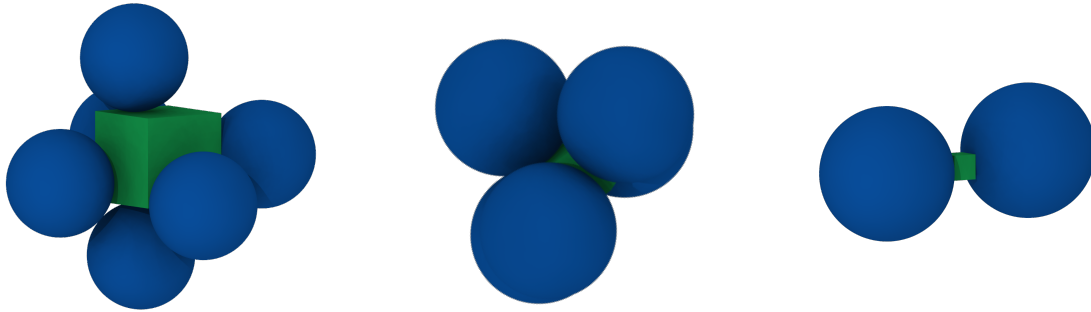


Figure S6: Typical configurations as obtained from the random parking algorithm based on selecting a random site for spheres attached to the surface of a cube for different size ratios  $\alpha = 1.2, 2.4$  and  $5.4$ .

### 3 Effect of varying the inverse Debye screening length

Here, we analyze the effect of changing the inverse Debye screening length  $\kappa$  from  $20\sigma^{-1}$  ( $0.1 \text{ nm}^{-1}$ ), the one reported in the main text, to  $10\sigma^{-1}$  and  $50\sigma^{-1}$ , corresponding approximately to  $0.05 \text{ nm}^{-1}$  and  $0.3 \text{ nm}^{-1}$  respectively. This is shown in Figure S7 in terms of the average cluster size distribution. We can observe that changing the electrolyte concentration has only minor effects on the overall distribution. At longer screening lengths,  $\kappa=10 \sigma^{-1}$ , the average cluster size is slightly shifted towards larger values at intermediate size ratios. While at short screening lengths the opposite effect is observed.

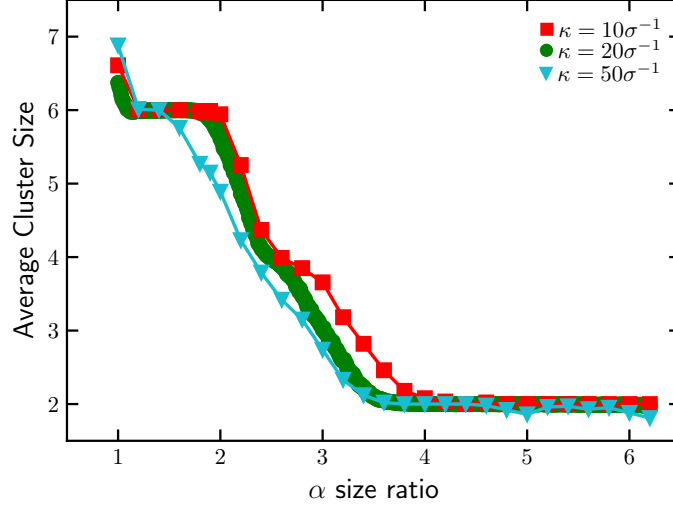


Figure S7: Average cluster size distribution as a function of the sphere-to-cube size ratio  $\alpha$  for different values of the inverse Debye screening length  $\kappa$  at fixed  $\epsilon_{cs} = 15$ .

#### 4 Monte Carlo simulations with Yukawa interactions

In the main text, we show results as obtained from Monte Carlo simulations using screened Coulomb interactions between the satellite spheres and the cubes with interaction strengths  $\epsilon_{cs} = 15$  and  $\epsilon_s = 10$ . In Figure S8, we show the average cluster sizes, i.e. average number of particles attached to the central cube, as a function of  $\alpha$  for varying values of  $\epsilon_{cs}$ . We observe that the average cluster size is affected only in a limited way by a change of the interaction strength  $\epsilon_{cs}$ .

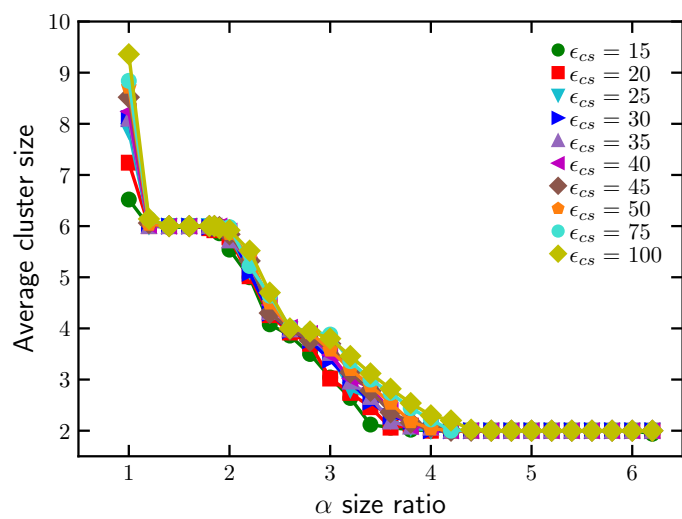


Figure S8: Average number of particles attached to the central cube as a function of size ratio  $\alpha$  for varying values of the interaction strength  $\epsilon_{CS}$ .

## 5 Unfused dried colloidal molecules

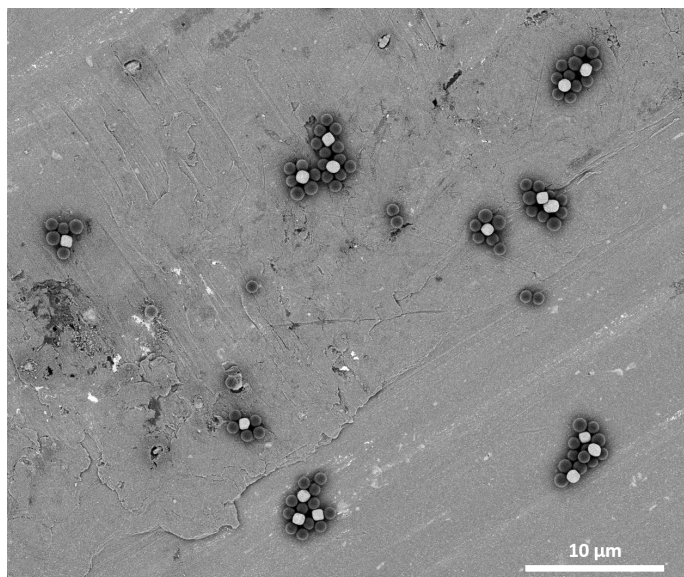


Figure S9: Scanning electron microscopy image of dried-disengaged colloidal molecules assembled from polystyrene spheres and hematite cubes.

## 6 Supplementary Movies

Movie S1: Show the real time 7.8 per sec frame rate bright-field microscope video of colloidal molecules made of polystyrene-hematite particles for  $\alpha = 1.20$ .

Movie S2: Show the real time 7.6 per sec frame rate bright-field of microscope video of colloidal molecules made of polystyrene-hematite particles for  $\alpha = 1.85$ .

Movie S3: Show the real time 9.8 per sec frame rate bright-field microscope video of colloidal molecules made of polystyrene-hematite particles for  $\alpha = 2.40$ .

Movie S4: Show the real time 9.8 per sec frame rate bright-field microscope video of colloidal molecules made of polystyrene-hematite particles for  $\alpha = 5.48$ .

Movie S5: Show the real time 8.4 per sec frame rate bright-field microscope video of colloidal molecules made of silica-hematite particles for  $\alpha = 1.16$ .

Movie S6: Show the real time 11.0 per sec frame rate bright-field microscope video of colloidal molecules made of silica-hematite particles for  $\alpha = 1.90$ .

Movie S7: Show the real time 7.8 per sec frame rate bright-field microscope video of colloidal molecules made of silica-hematite particles for  $\alpha = 2.48$ .

Movie S8: Show the real time 25.6 per sec frame rate bright-field microscope video of colloidal molecules made of silica-hematite particles for  $\alpha = 5.56$ .